Finite element modeling of guyed backspars in cable logging

Albert Saravi and C. Kevin Lyons

Abstract: In this study a finite element model of a backspar system was developed with three guylines opposing the skyline strap tension. In this paper the allowable skyline strap tension is the tension in the skyline strap that results in the maximum normal stress on a transverse cross section of the tree being equal to an assumed allowable stress. An iterative routine was developed to find the allowable skyline strap tension, and this routine was found to converge rapidly from initial values that were below and above the allowable skyline strap tension. Two algorithms were developed for finding the maximum normal stress on a transverse cross section of a tree, method 1 and method 2. If the plane that the tree displaced in was known a priori, then method 2 could be used, and it was found to be less sensitive to mesh coarseness. If the plane that the tree displaced in was not known a priori, then method 1 had to be used with a less coarse mesh. It was found that the stress concentrations due to simplified cable connections were not significant for rigging configurations that allowed a larger rigging point displacement. The rigging configurations that allowed larger rigging point displacements have stress fields that are dominated by bending, while for rigging configurations that allow only small rigging point displacements, the stress fields are dominated by axial compression.

Résumé : Dans cette étude, un système de mât de queue avec trois haubans pour absorber la tension de la sangle du câble porteur a été modélisé par la méthode des éléments finis. Dans cet article, la tension de la sangle du câble porteur permise correspond à la tension dans la sangle engendrée par la contrainte normale maximale en section transversale de l'arbre. Cette tension correspond à la contrainte acceptable présumée. Une routine itérative a été développée afin de trouver la tension permise de la sangle du câble porteur. Cette routine converge rapidement à partir de valeurs initiales inférieures et supérieures à la tension permise. Deux algorithmes ont été développés pour trouver la contrainte normale maximale en section transversale d'un arbre : la méthode 1 et la méthode 2. Lorsque la zone de débardage est connue a priori, la méthode 2 peut être utilisée. Cette dernière s'est montrée moins sensible à la taille du maillage. Cependant, si la zone de débardage n'est pas connue a priori, la méthode 1 doit alors être utilisée avec un maillage plus fin. Les résultats montrent que la concentration des contraintes dues aux connections simplifiées des câbles n'est pas significative pour les configurations qui permettent de couvrir une plus grande surface. Les configurations de câblage qui permettent de couvrir de plus grandes zones ont des champs de contraintes dominés par le cintrage alors que les configurations de câblage couvrant de plus petites zones ont des champs de contraintes dominés par la compression axiale.

[Traduit par le Rédaction]

1. Introduction

Common skyline logging systems employ a bicable ropeway (Schneigert 1966), which as the name suggests consists of two cables, a skyline and a mainline. The logs are suspended from a carriage that is pulled along the skyline by the mainline, where the skyline is the carrying cable and the mainline is the hauling cable. The function of hauling logs from the cutblock to the roadside is termed yarding; the machine containing the winch set for the cables and usually a tower to support the skyline is called the yarder.

Received 22 April 2003. Accepted 17 October 2003. Published on the NRC Research Press Web site at http://cjfr.nrc.ca on 16 April 2004.

A. Saravi. Electrical and Computer Engineering Department, The University of British Columbia, 2356 Main Mall, Vancouver, BC V6T 1Z4, Canada.
C.K. Lyons.[1] Department of Forest Resource Management, The University of British Columbia, 2424 Main Mall, Vancouver, BC V6T 1Z4, Canada.

[1]Corresponding author (e-mail: kevlyons@interchange.ubc.ca).

The skyline is a wire rope suspended between two or more points (Conway 1976). The suspension points may be the yarder, trees, or stumps. The advantage of using a skyline logging system is that there is greater control over the logs when yarding, and it is possible to either partially or fully suspend the logs to minimize ground disturbance. To realize this advantage it is necessary to maintain a minimum clearance between the ground and the carriage. In some situations it is necessary to support both ends of the skyline to maintain adequate clearance. Backspars are often used to support the end of the skyline opposite from the yarder (Fig. 1).

The structural behavior of backspars is of interest because they can limit the capacity of the logging system. The performance of the rest of the skyline logging system is not sensitive to lateral displacement of the backspar. The displacement of the backspar becomes important when geometric nonlinear effects are present. The geometric nonlinear effects with regard to the backspar are often termed the *P*–delta effect.

Stalnaker and Harris (1989) discuss the *P*–delta effect in beam column design, where there is a moment magnification

 doi: 10.1139/X03-250

Fig. 1. Diagram of the backspar.

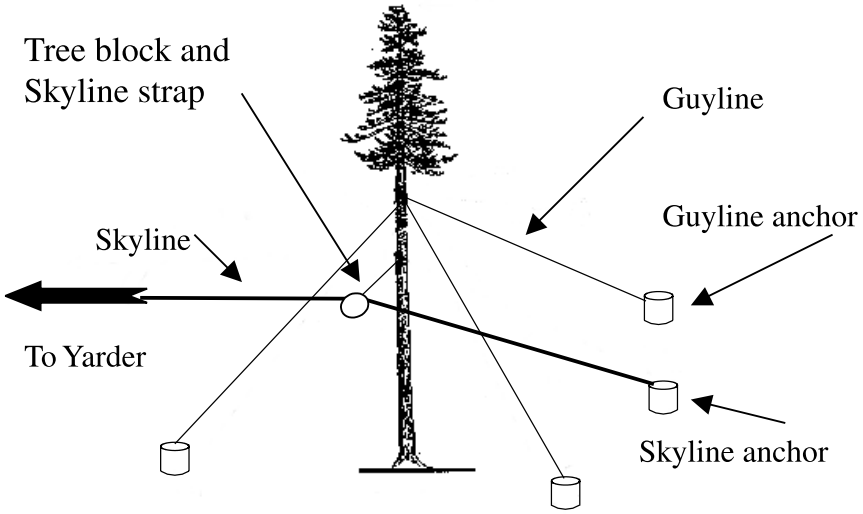

from the product of the vertical load (P) and the lateral deflection (delta). The backspar also has a flexible base, which can be represented as a rotational spring (Pyles 1987). The interaction of the nonlinear restraining force supplied by the guylines, the P–delta effect of the column, and the rotational stiffness of the base may combine to produce a complicated displacement field in the backspar.

Lyons (1997) used elementary beam theory to estimate the mechanical stresses in backspars. This study indicated that compression parallel to the grain would be the limiting stress; however, the calculated maximum stress was located farther down the backspar than where other backspars were observed to have failed. Ammeson et al. (1988) demonstrated that the geometric nonlinear effects in the structural analysis of backspars could be modeled in a finite element model (FEM). Ammeson et al. (1988) used beam elements to model the backspar, where the bending component of the stiffness matrix used in the model was derived from the Bernoulli–Euler law of elementary bending theory.

Connor (1989) studied the stress distribution in backspars rigged for experimental purposes and used Ammeson's model to predict the displacement of the rigging point on the backspar. Connor compared the predicted displacement of the rigging point with the actual displacement of test backspars and found agreement to within a few centimetres. However, Connor's results also showed that the maximum stress in compression was near the base of the backspar. Neither Connor (1989) nor Lyons (1997) measured backspars that were loaded to failure. It is possible that in these studies the applied loads were not sufficient to produce a noticeable P–delta effect.

Pyles and Lyons (2001) proposed using the allowable normal stress on a transverse cross section of a backspar as a design limit for an unguyed backspar. With this design limit, it was possible to determine allowable skyline strap tensions for given rigging configurations. A similar design limit will be used in this study.

In this study the phenomenon of interest is the allowable tension in the skyline strap given the geometry and material properties of the tree used as the backspar; the end locations, length, and material properties of the guylines; and an assumed allowable stress on a transverse cross section of the backspar. It is hypothesized that this restricted problem is strongly dependent on the direction of the skyline strap, the geometry of the backspar, and the length and the end locations of the guylines.

In this study the allowable stress on a transverse cross section of the backspar is assumed to be the allowable stress in bending for northern Douglas-fir (*Pseudotsuga menziesii* (Mirb.) Franco) (1.103×10^7 Pa) (American Forest and Paper Association 1997). The tension in the skyline strap that produces the allowable stress in the backspar will be found through structural analysis of the system. This procedure will result in an allowable skyline strap tension for a given rigging configuration and a given allowable stress in the backspar. Thus, it will be possible to consider the effect on the allowable skyline strap tension from parameters such as the direction of the skyline strap, the geometry of the backspar, the length of the guylines, and the end locations of the guylines.

2. Objectives

In this study a finite element model (FEM) of a backspar system will be developed with three guylines opposing the skyline strap tension. This study will consider the scenario where the initial tension of the second guyline varies from the initial tensions of the other two guylines. The FEM will be constructed using the commercially available software ANSYS® (ANSYS Inc., Canonsburg, Pa.). The FEM will consider the self-weight of the tree, the actual taper of the tree as predicted by taper equations, the flexible base of the tree, the nonlinear load response of the guylines to displacement, and the nonlinear load response of the backspar due to the P–delta effect. Once the model is developed, two solution algorithms for finding the allowable skyline strap tension will be compared.

3. Tree bole elastic coefficients

To use a FEM of a backspar it is necessary to identify the appropriate material model and the type of elements to be

Fig. 2. Cylindrical coordinate axes in a section of a tree.

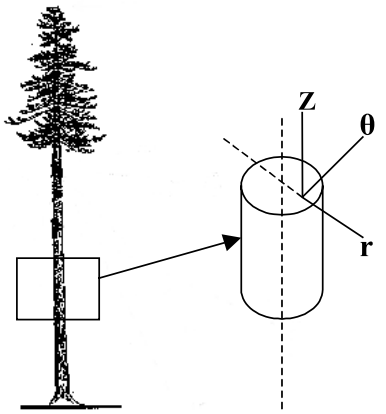

used. For example, Pellicane and Nilson (1993) used a detailed solid element FEM to model the effects of grain pattern around knots in wooden poles, while Ammeson et al. (1988) used beam elements to model the displacement of a backspar. Bodig and Jayne (1993) describe a cylindrical section of a tree as being an orthotropic material with cylindrical anisotropy, where the axes of symmetry are the long axis Z, the radial axis r, and the tangential axis θ (Fig. 2). If a cylindrical section of a tree is consider orthotropic in cylindrical coordinates, then it will not be possible to estimate the normal stresses or the shear stress in the $r\theta$ plane using elementary beam theory.

Lyons et al. (2002*a*, 2002*b*) considered the problem of a cylindrical section of a tree as a Relaxed Saint-Venant's Problem. When posing the problem in this form, it is still assumed that plane sections remain plane; however, it is possible to consider the orthotropic properties of trees. Lyons et al. (2002*a*, 2002*b*) determined that the normal stress in the r direction (S_r), the normal stress in the θ direction (S_θ), and the shear stress in the $r\theta$ plane ($S_{r\theta}$) must all be equal to zero for loads independent of Z.

It is desirable to use a material description that is similar to the actual material in case there are unexpected interactions between the strains and the stresses; however, the FEM software used in this study is not able to consider a material that is orthotropic with respect to the cylindrical coordinates. Lyons et al. (2002*a*) found for the homogeneous case that it is acceptable to model the tree as if it were transversely anisotropic. Therefore, in this study a solid element will be used that is able to consider the tree as transversely anisotropic.

The engineering constants for wood vary both within a tree and among trees; however, averaged values are reported in the literature. Table 1 presents the values for the engineering constants published by Bodig and Jane (1993) for coastal Douglas-fir at 12% moisture content.

To simplify the properties of the wood so that it may be modeled as a transversely isotropic material, the elasticity tensor must be made symmetric and the following must be true:

$$[1] \qquad E_\theta = E_r, \qquad G_{rZ} = G_{\theta Z}, \qquad \nu_{rZ} = \nu_{\theta Z}$$

Here, E_θ and E_r are the Young's modulus in the r and θ directions, G_{rZ} and $G_{\theta Z}$ are the shear modulus in the rZ and θZ planes, and ν_{rZ} and $\nu_{\theta Z}$ are the Poisson's ratios linking, respectively, the normal stress in the r and θ directions to the normal strain in the Z direction.

Table 1. Engineering constants for coastal Douglas-fir (Bodig and Jane 1993).

E_Z (Pa)	1.476×10^{10}
E_θ (Pa)	6.288×10^{8}
E_r (Pa)	9.818×10^{8}
$G_{\theta Z}$ (Pa)	7.426×10^{8}
G_{rZ} (Pa)	7.998×10^{8}
$G_{\theta r}$ (Pa)	8.508×10^{7}
ν_{Zr}	0.383
$\nu_{Z\theta}$	0.340
$\nu_{r\theta}$	0.432
ν_{rZ}	0.022
$\nu_{\theta r}$	0.308
$\nu_{\theta Z}$	0.017

Note: E, Young's modulus; G, shear modulus; ν, Poisson's ratio. Subscripts: Z, long axis; r, radial axis; θ, tangential axis.

Table 2. Engineering constants for coastal Douglas-fir averaged so that it can be modeled as a transversely isotropic material.

E_Z (Pa)	1.476×10^{10}
E_θ (Pa)	8.053×10^{8}
E_r (Pa)	8.053×10^{8}
$G_{\theta Z}$ (Pa)	7.712×10^{8}
G_{rZ} (Pa)	7.712×10^{8}
$G_{\theta r}$ (Pa)	8.508×10^{7}
ν_{Zr}	0.362
$\nu_{Z\theta}$	0.362
$\nu_{r\theta}$	0.375
ν_{rZ}	0.020
$\nu_{\theta r}$	0.375
$\nu_{\theta Z}$	0.020

Note: E, Young's modulus; G, shear modulus; ν, Poisson's ratio. Subscripts: Z, long axis; r, radial axis; θ, tangential axis.

The elasticity tensor will be made symmetric by averaging the coefficients that are above and below the diagonal in the elasticity tensor. The elasticity tensor will be made transversely isotropic by averaging the coefficients in eq. 1 (Table 2).

4. Tree base elastic coefficients

Pyles (1987) found that trees have flexible bases, which can be represented as rotational springs. However, a rotational spring only rotates about a single axis. Therefore, a short cylinder will be used to represent the flexible base of the tree (Fig. 3). The cylinder will be hollow to reduce the number of elements required to form it in the FEM.

The maximum length of the cylinder that forms the base of the tree will be estimated using beam theory. The length of the cylinder will be selected so that a shear stress applied

Fig. 3. Free body diagram of base cylinder.

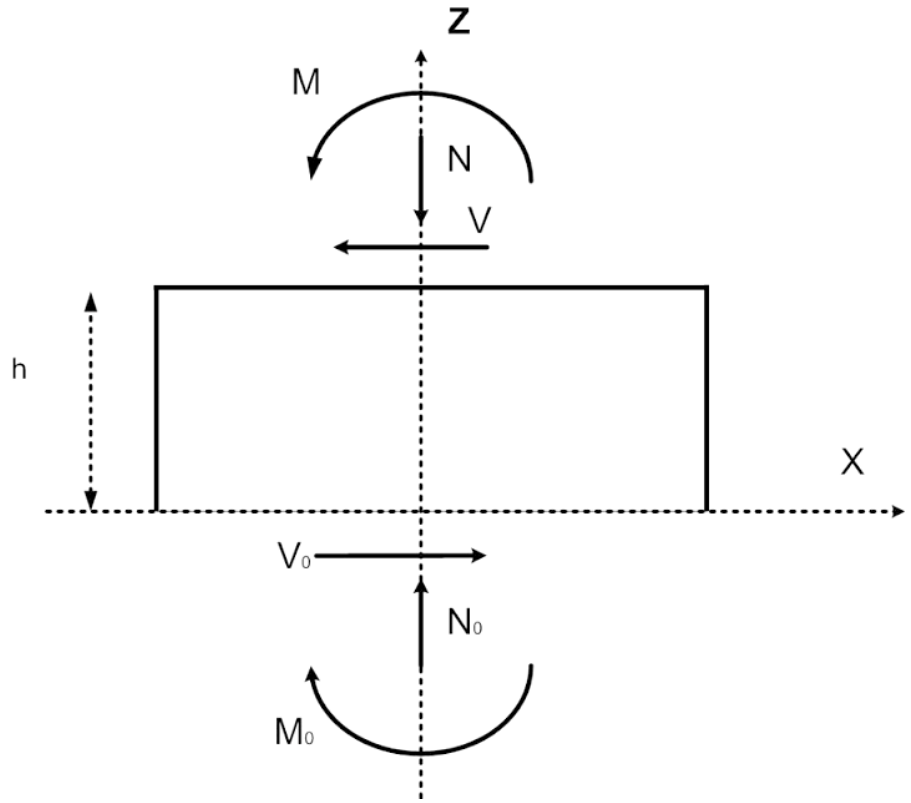

to the top of the cylinder will produce a negligible moment on the base of the cylinder when compared with the moment applied to the top of the cylinder. Once the length of the cylinder has been selected, the modulus of elasticity of the cylinder can be determined so that the rotation of the top of the cylinder for a given moment is equivalent to the rotation given by Pyles (1987) for the same moment.

Let V, V_o, and V' be, respectively, the shear force applied to the top of the cylinder, the shear force applied to the base of the cylinder, and the shear force on an arbitrary cross section. Let M, M_o, and M' be, respectively, the moment applied to the top of the cylinder, the moment applied to the base of the cylinder, and the moment on an arbitrary cross section. Let N, N_o, and N' be, respectively, the normal force applied to the top of the cylinder, the normal force applied to the base of the cylinder, and the normal force on an arbitrary cross section.

Assume the origin is centered at the base of the cylinder, with the Z axis oriented up the cylinder, and the positive X axis in the direction of the shear force applied to the top of the cylinder. Assuming the shear force acts in the X direction is acceptable, since the cylinder has circular cross sections. The moment equation for the cylinder is

$$[2] \qquad M' = M_o - V_o Z$$

Here, $M_o = Vh + M$, and $V_o = V$, where h is the length of the cylinder.

From beam theory the displacement of the end of the cylinder is given by

$$[3] \qquad \frac{d^2v}{dZ^2} = \frac{M'}{EI}$$

Substitute the moment equation (eq. 2) into the differential equation for beam deflection (eq. 3) and then integrate once to get the slope of the beam at Z. Note, since the base of the cylinder is fixed, the constant of integration is zero. Set $Z = h$, then

$$[4] \qquad \frac{dv(h)}{dZ} = \frac{1}{EI}\left(Vh^2 - \frac{Vh^2}{2} + Mh\right)$$

Recall that h will be selected so that the shear component of the rotation is negligible. Therefore, select h so that the rotation of the top of the cylinder resulting from the shear force acting on the top of the cylinder is at least two orders of magnitude smaller than the rotation of the top of the cylinder due to the moment applied to the top of the cylinder.

$$[5] \qquad \left|\frac{Vh^2}{2}\right| << |Mh|$$

Then the equation for the rotation of the end of the cylinder becomes

$$[6] \qquad \frac{dv(h)}{dZ} = \frac{1}{EI}(Mh)$$

Pyles (1987) describes the base of a tree as a rotational spring with the spring constant (in kilonewton metres per degree):

$$[7] \qquad K = 4.13E - 4(ID_{1.5})^{3.65}$$

Fig. 4. Finite element model of tree base.

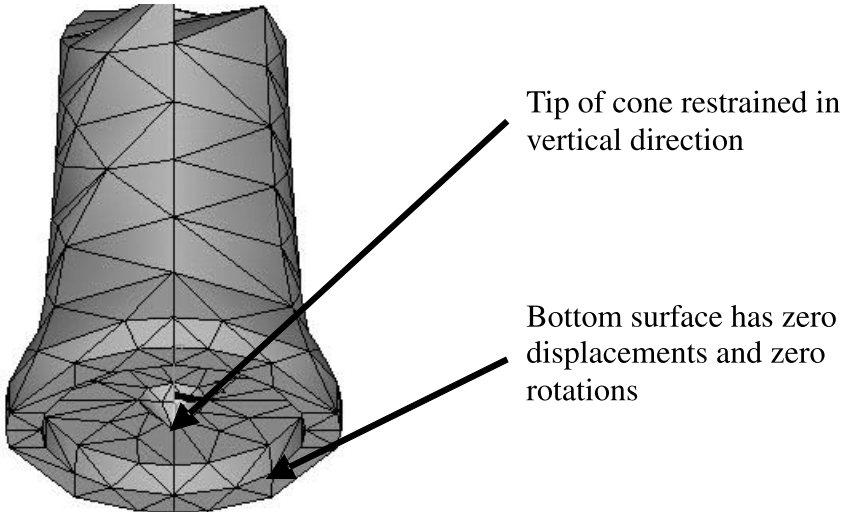

Rewrite eq. 7 with units of newton metres per rad, then

$$[8] \qquad R = 23.6649(ID_{1.5})^{3.65}$$

The moment of inertia, I, for a circular cylinder is

$$[9] \qquad I = \frac{\pi}{64}(D^4 - d^4)$$

where D is the outside diameter of the cylinder in metres, and d is the inside diameter of the cylinder in metres.

Set the slope of the end of the cylinder equal to 1 radian in eq. 6. Recall the spring constant is now in newton metres per rad, which is moments per radians. Therefore, reorganize the slope equation, substitute eq. 8 into this, and solve for the required E:

$$[10] \qquad E = 482.097\frac{(ID_{1.5})^{3.65}h}{D^4 - d^4}$$

Thus, the length of the cylinder will be selected so that the left-hand side of eq. 5 is at least two orders of magnitude smaller than the right-hand side, and eq. 10 will be used to estimate the required modulus of elasticity of the cylinder. The actual values of h and E will be determined during trial runs of the model.

The intent of supporting the tree with an elastic foundation was to approximate the rotational spring identified by Pyles (1987); however, the elastic base will also allow vertical motion of the base of the tree. Therefore, the base of the tree will be restrained from vertical translation by an inverted cone with a modulus of elasticity equal to $E_{cone} = E_Z \times 10\,000$ (Fig. 4). The base of the cone is attached to the center of the base of the tree, and the tip of the cone is restrained from vertical translation, but is free to rotate. The shape of a cone was selected to reduce the number of elements required to form it, to reduce the stress concentration on the base of the tree, and to allow rotation by essentially making the tip of the cone a ball joint.

5. FEM of the tree bole

The diameter of the tree was calculated using a taper equation introduced by Kozak (1988). This taper equation gives the diameter inside the bark as a function of the vertical distance up the tree. The taper equation requires the diameter at breast height (DBH, the diameter of the tree outside the bark at 1.3 m) and the total height of the tree:

$$[11] \qquad d_i = a_0 D^{a_1} a_2^D X^{b_1 Z^2 + b_2 \ln(Z+0.001) + b_3\sqrt{Z} + b_4 e^Z + b_5 (D/H)}$$

where

$$Z = h_i/H, \qquad X = \left[1 - \sqrt{(h_i/H)}/\left(1 - \sqrt{p}\right)\right]$$

and D is DBH, h_i is the height up the tree, d_i is the diameter inside the bark at h_i, H is the total height of the tree, and $p = 100(H_1/H)$, where H_1 is the height of the inflection point from the ground. The values of the coefficients required in eq. 11 for Douglas-fir are listed in Table 3

The total height of the tree (H) will be 30 m for all the scenarios in this study. It is assumed that convergence problems in the FEM or unexpected responses of the backspar to the applied loads will be more likely when the nonlinear effects are larger. Therefore, the tree modeled in this study will be slender to consider a larger P–delta effect. The tree considered in this study will have DBH = 35 cm. Note, the total height (H) is required for the taper equation; however, the tree will be topped at 16 m and rigged (that is the cables will be attached) at 15 m.

The bole of the tree was modeled using ANSYS® SOLID92 elements. As stated in section 3, the tree was assumed to be transversely isotropic (Table 2). Bodig and Jane (1993) give the density of coastal Douglas-fir (at 12% moisture content) as $\rho = 450$ kg/m^3.

The base and the bole of the tree were meshed using the ANSYS® smart meshing option, with mesh coarseness ranging from 10 (most coarse) to 4 (less coarse). Note, the ANSYS® license used in this study was limited to 100 000 nodes. The limit in the number of nodes that could be used

Table 3. Taper equation coefficients from eq. 11 (Kozak 1988).

a_0	1.024 53
a_1	0.888 09
a_2	1.000 35
b_1	0.950 86
b_2	–0.180 90
b_3	0.614 07
b_4	–0.351 06
b_5	0.056 86
p	0.25

Table 4. Properties of the guyline cable.

Force per unit length (N/m)*	10.5
Diameter (m)*	0.0159
Cross-section area (m^2)*	1.986×10^{-4}
Density (kg/m^3)*	5389
Modulus of elasticity (Pa)†	9.6521×10^{10}

*Bethlehem Wire Rope (Williamsport Wirerope Works, Inc., Williamsport, Pa., http://www.wwwrope.com), 16.0 mm diameter, 6X19 IWRC.
†British Ropes (1955), 6X19 IWRC.

in this study resulted in mesh coarseness 4 being the finest mesh that could be used.

6. FEM of the guylines

The guylines used to restrain backspars have significant sag when the backspar is initially rigged. When the backspar is loaded with the skyline strap, the rigging point may displace laterally until the sag in the guylines is removed. The lateral displacement of the rigging point creates a significant *P*–delta effect; therefore, it is important to be able to consider the sag in the guylines.

The properties of the guyline cables used in this study are listed in Table 4. The cables are assumed to be linearly elastic, unable to support internal moments, and to have significant self-weight. The ANSYS® LINK10 element is able to consider these assumptions for the cable, and when the tension-only option is used, the stiffness is removed if the cable goes into compression.

The procedures used to model the guylines are as follows. For a given guyline the following are known: the rigging point location, the guyline anchor location, and the initial guyline tension at the lower end. Carson's (1977) catenary equations for a single cable segment were used to calculate the initial guyline length given the initial tension at the lower end.

Using the initial length of the guyline, a line was constructed and meshed with the upper end attached to the backspar at the rigging point and the lower end located past the anchor position. The lower end was then displaced to the guyline anchor location. Displacing the lower end of the cable to the anchor location allows ANSYS® to solve for the final node locations of the elements within the guyline. This procedure was found to be sensitive to the coarseness of the meshing; however, Fig. 5 shows that the model stabilizes once 60 elements are used to model a guyline. Therefore, each of the guylines was divided into 100 elements.

Fig. 5. Sensitivity of guylines to meshing coarseness (rigging height = 15 m, radial distance = 35 m, initial tension = 300 N).

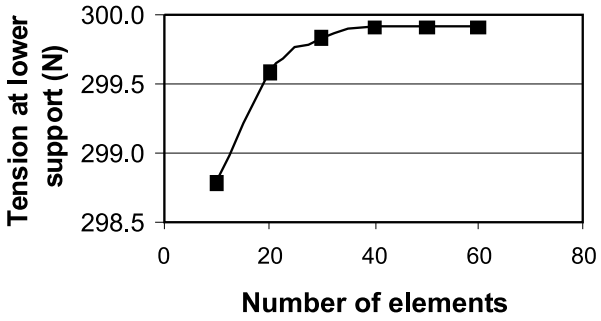

7. Model parameters and solution methods

7.1. Model parameters

This study will consider the scenario where the initial tension of the second guyline varies from the initial tensions of the other two guylines. The second guyline can be considered the middle guyline (Fig. 6). As shown in Fig. 6, the skyline strap is assumed to act in the *XZ* plane. The skyline strap angle is described as the angle between the vertical and the skyline strap (Fig. 7). The geometry and tension values considered in this project are listed in Table 5.

7.2. Algorithm for finding the allowable skyline strap tension

The allowable tension in the skyline strap (T_{all}) is defined as the tension in the skyline strap that results in the maximum compressive stress on a transverse cross section being equal to the allowable compressive stress for the backspar (σ_{all}). In the model developed for this study, the connections for the guylines and the base were simplified. Specifically, the node on the tip of the cone that limits the vertical motion of the tree base and the nodes to which the guylines and the skyline strap are attached experience stress concentrations because of the application of forces on single points. Lyons (1997) noted that backspars commonly failed in the middle third of the tree. Therefore, to avoid the stress concentrations resulting from the connection simplifications, only the region from 1 to 14 m above the base was considered. Let this region be called *B* (Fig. 8).

To find the allowable skyline strap tension, a first guess was made at the skyline strap tension (T_o). Using this first guess, the FEM was run, and the greatest stress in compression on a transverse cross section (σ_{max}) was found within *B*. The model checks whether σ_{max} is within ±1% of the allowable stress value for the backspar. If σ_{max} is not within ±1% of σ_{all}, then T_o is corrected as follows:

$$[12] \quad T_{corr} = \left(\frac{\sigma_{all} - \sigma_{max}}{\sigma_{max}} + 1 \right) T_o$$

Fig. 6. Guyline anchor location.

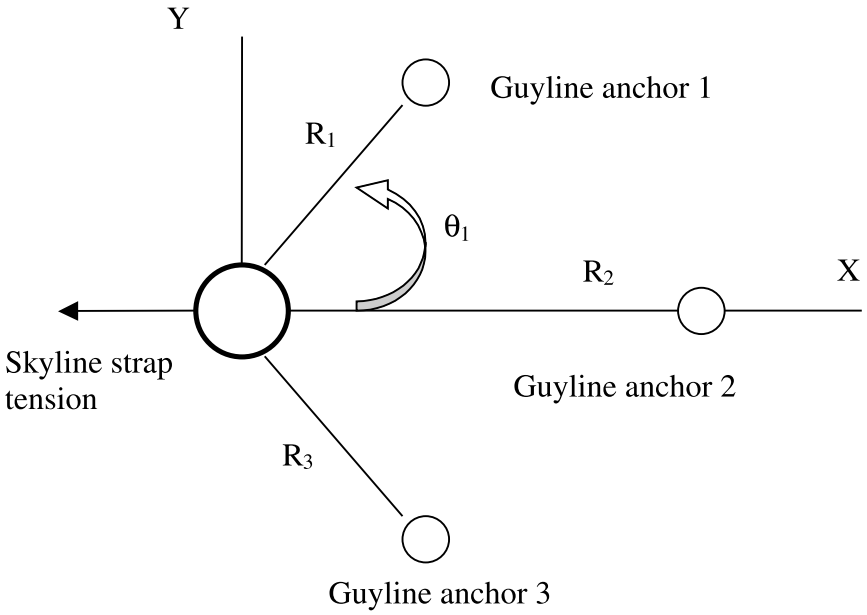

Fig. 7. Skyline strap angle.

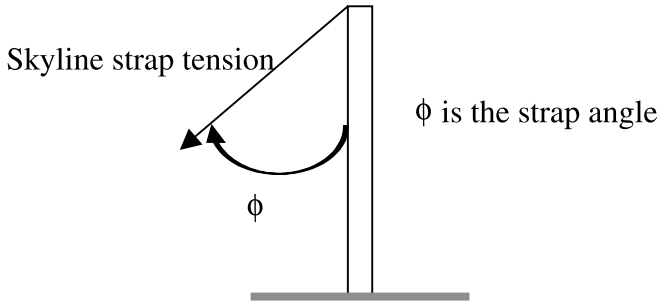

The model is then run using T_{corr}. This procedure is repeated until σ_{max} is within ±1% of σ_{all}. The T_{corr} that results in σ_{max} being within ±1% of σ_{all} is called T_{all}.

7.3. Methods for determining σ_{max}

Two methods for determining σ_{max} were considered in this study. The first method, method 1, searched for σ_{max} anywhere in *B*. Method 1 is the preferred method when the plane that the backspar will displace in is not known a priori.

The ANSYS® SOLID92 element is a 10-node tetrahedron, with 4 nodes located at the corners and 6 nodes located midpoint between the corners. During the meshing process the meshing algorithm in ANSYS® attempts to form the backspar, which is a tapered column with circular cross sections, using the SOLID92 elements. Since the SOLID92 element has straight sides, the meshed volume is not exactly the same as the original backspar volume (Fig. 9).

Consider the problem where the stresses are dominated by bending loads, with the lateral displacements occurring in the *XZ* plane. In Fig. 9, nodes α and γ, which would be corner nodes of some elements, fall on the boundary of the actual backspar volume, with node α being located at the point where the maximum compressive load on the transverse cross section occurs.

If the hexagon in Fig. 9 was rotated 30° clockwise, then the meshing algorithm would again put corner nodes α and γ on the actual boundary of the backspar. However, in the rotated Fig. 9 the meshed volume would be oriented so that it is less efficient at supporting the bending loads and it would have a lower second moment of inertia. In fact the ANSYS® meshing algorithm is alternating the patterns found in Fig. 9

Table 5. Parameter values.

Parameter	Values that will be considered
Guyline size (mm)	15.9
Skyline strap angle, ϕ, (°)	5
Guyline 1	
Radial distance, r_1, (m)	25
Polar angle, θ_1, (°)	45
Initial tension, IG_1, (N)	600, 1000
Guyline 2	
Radial distance, r_2, (m)	25
Polar angle, θ_2, (°)	0
Initial tension, IG_2, (N)	$0.5 \times IG_1$, IG_1, $1.5 \times IG_1$
Guyline 3	
Radial distance, r_3, (m)	25
Polar angle, θ_3, (°)	–45
Initial tension, IG_3, (N)	$IG_3 = IG_1$
Tree DBH (cm)	35
Tree height (m)	30
Rigging height (m)	15
Allowable normal stress on a transverse cross section (Pa)	1.103×10^7

Fig. 8. Region *B* of the backspar. See text for definition of region *B*.

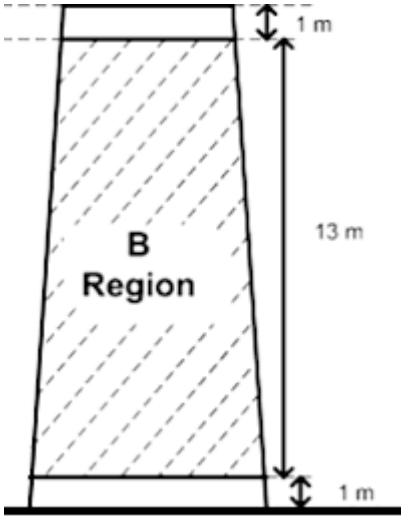

Fig. 9. Backspar cross section with meshing error due to element shape.

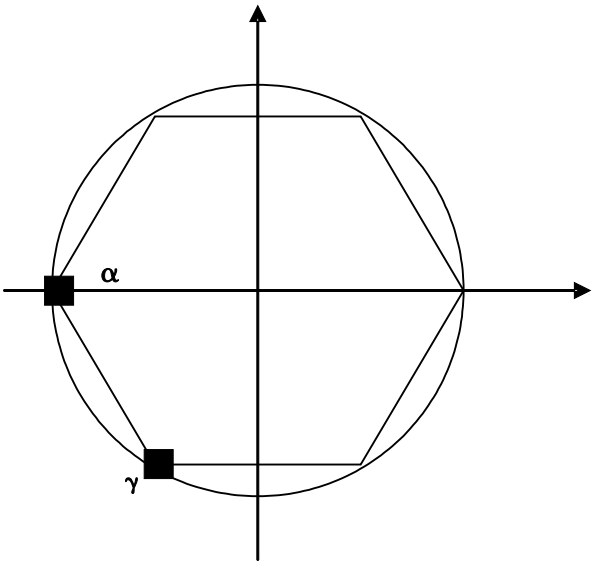

and the rotated Fig. 9, with the result that a search for σ_{max} anywhere in *B* will find higher stresses on cross sections similar to the rotated Fig. 9. Finding σ_{max} at a higher stress that is a function of the meshing algorithm will result in an underestimation of T_{all}.

The underestimation of T_{all} will, of course, decrease as the coarseness of the mesh decreases; however, this is at the cost of longer solution times. Therefore, a second method for finding σ_{max} was developed. The second method considered in this study, method 2, is preferable when the plane that the backspar will displace in is known a priori. Method 2 searches for σ_{max} on corner nodes that are nearest to the distal fiber in the plane that the backspar displaces. Method 2 forces the algorithm to pick nodes that are near the lateral surface of *B*. Since the problem, as noted by Lyons (1997), is strongly affected by bending, it is expected that σ_{max} should occur on the lateral surface of *B*. In addition, method 2 forces the algorithm to search for σ_{max} on cross sections similar to those found in Fig. 9, because this is the only time that corner nodes are located on the distal fiber. Searching for σ_{max} on cross sections similar to those in Fig. 9 results in the algorithm avoiding the higher stresses resulting from meshing, and so the algorithm will be less sensitive to mesh coarseness.

Table 6. Rigging configuration naming codes.

Name code	IG_1 (N)	ϕ (°)	IG_2/IG_1	r_2 (m)	DBH (cm)
51621	1000	5	1.5	25	35
51421	1000	5	1.0	25	35
51221	1000	5	0.5	25	35
31621	600	5	1.5	25	35
31421	600	5	1.0	25	35
31221	600	5	0.5	25	35

Note: IG_1, initial tension in guyline 1; IG_2, initial tension in guyline 2; ϕ, skyline strap angle; r_2, radial distance in guyline 2; DBH, diameter at breast height.

8. Analysis

8.1. Rigging configurations

The naming codes for the rigging configuration considered in this study are presented in Table 6. The definition of the numbers in the naming codes are as follows: the first number is the code for the initial tension of guyline 1, the second number is the code for the skyline strap angle, the third number is the code for the ratio of the initial tension in guyline 2 and guyline 1, the fourth number is the code for the radial distance of the guyline 2 anchor from the base of the backspar, and the final number is the code for the DBH of the backspar.

8.2. Stress concentrations at the rigging point and at the base

Recall the vertical displacement of the base of the tree was restrained with a cone. It was found, even for the trees with the highest cable loads applied to them, that the stress concentrations resulting from the cone at the base of the tree never extended up into the region *B*.

The guylines and skyline strap were each connected to individual nodes on the tree; these nodes are located on the boundary of the cross section at the rigging height (Fig. 6). Obviously this method of connecting the cables to the tree creates a stress concentration near the connection point. However, the stress concentrations resulting from the cable connections should diminish before the region *B* if the stress field is dominated by bending. If the stress field is dominated by bending, then the magnitude of the normal stress on a transverse cross section should be greatest along the distal fiber in the plane of bending. Figure 10 gives the normal stress on the transverse cross section at the distal fiber on the negative *X* axis, for the rigging case 51621, which has the highest allowable tension, and for the rigging case 31221, which has the lowest allowable tension.

In Fig. 10, rigging case 31221 is the case with the greatest amount of sag in the guylines. Greater sag in the guylines

Fig. 10. Compression stress (σ) at the distal fiber on the negative *X* axis from 1.0 to 14.5 m up the tree for the allowable tension in the skyline strap (T_{all}) and the guylines applied at 15 m.

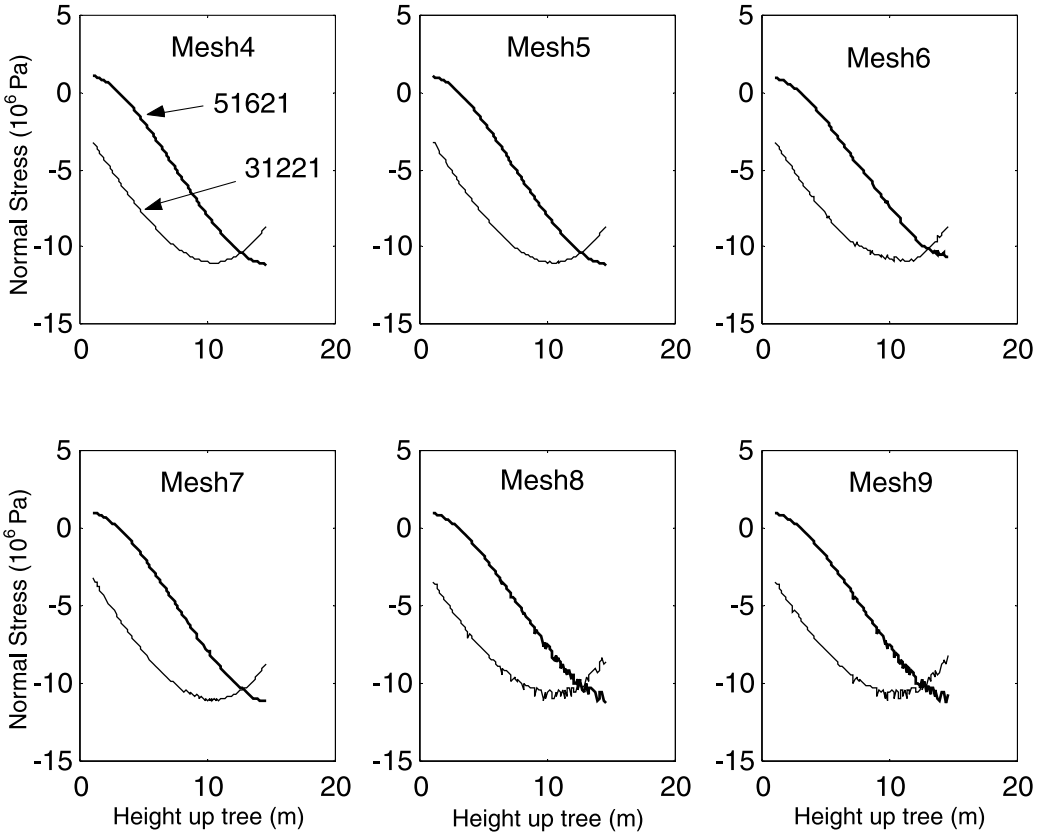

Fig. 11. Convergence of the initial guess at skyline strap tension (T_o) to the allowable tension in the skyline strap (T_{all}) for rigging case 31421 at mesh level 9.

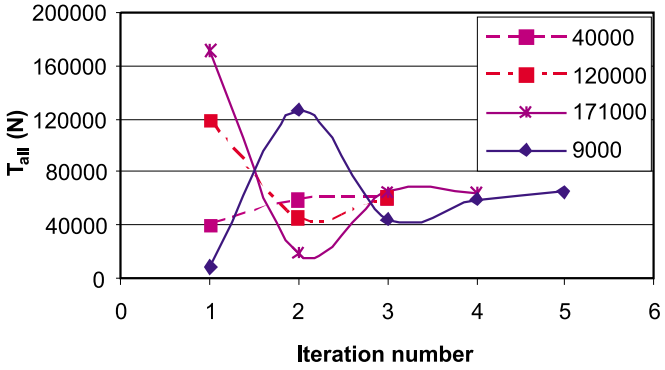

Fig. 12. Solution times as a function of mesh coarseness using method 2 (Pentium 4 processor, 1.6 GHz CPU, and 1 GB SDRAM).

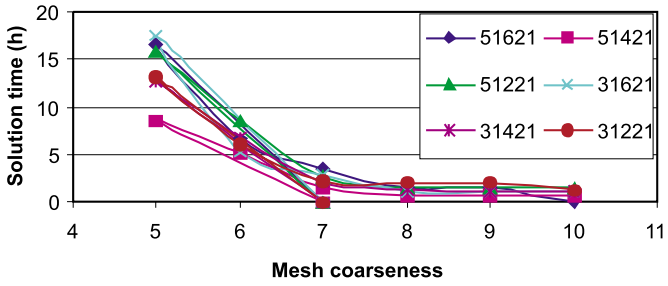

resulted in a larger displacement of the rigging point and, therefore, a larger *P*–delta effect. The large *P*–delta effect in rigging case 31221 results in the stress field being dominated by bending. The effect of bending on the stress field in rigging case 31221 is evident by the fact that the magnitude of the normal stress on the transverse cross section is greatest at about 10 m and then decreases towards the rigging point. Therefore, considering the region *B* to be the region where failure will occur is a good assumption.

In Fig. 10, rigging case 51621 is the case with the least amount of sag in the guylines. Less sag in the guylines resulted in a smaller displacement of the rigging point and, therefore, a smaller *P*–delta effect. The reduced *P*–delta effect allowed a greater T_{all} when it was assumed σ_{max} occurred in *B*. The greater T_{all} resulted in higher guyline loads, which, together with the reduced *P*–delta effect, resulted in a larger portion of the normal stress on the transverse cross section being a function of the axial load as opposed to bending. The effect of a having a larger portion of the normal stress on the transverse cross section being a function of the axial load can be seen in Fig. 10; in this case σ_{max} occurs at the upper boundary of *B*. Above the upper boundary of *B* it becomes difficult to tell where the stress concentrations due to the connections are significant given the very high axial load. This indicates that the stress concentrations due

Fig. 13. Allowable tension in the skyline strap (T_{all}) calculated using method 1.

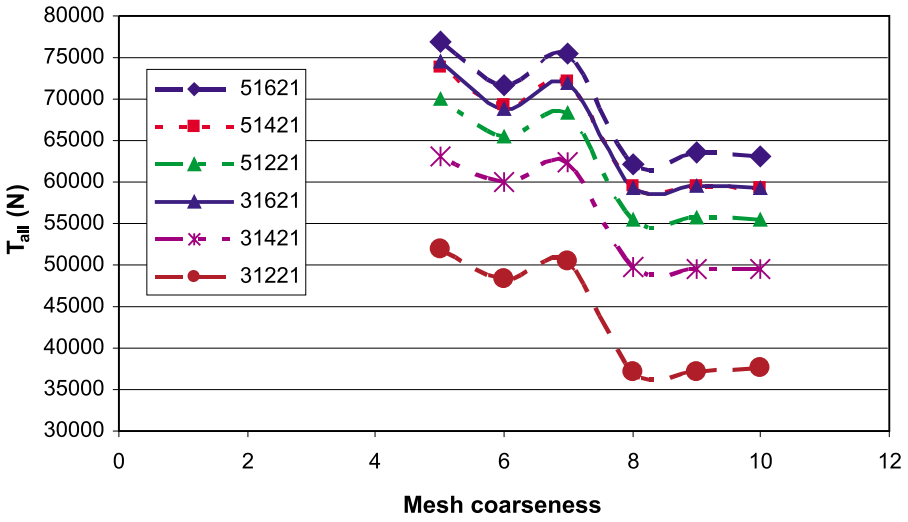

to the connections are very important for modeling stiff backspars where the stress field is not dominated by bending.

8.3. Convergence given T_o

It was found that the method used to find T_{all} as described in section 7.2 converged within two to four iterations (Fig. 11). For the rigging case considered in Fig. 11, the algorithm converged to about 62 000 N when T_o was between 9000 and 171 000 N. When T_o > 171 000 N, the tree is unable to support the initial guess at the skyline strap tension, and it buckles into a position that is physically impossible but that continues to support an ever increasing T_{corr}. Thus, the algorithm used to find T_{all} converges rapidly and reliably for a wide range of T_o values, with the upper bound for T_o being close to the buckling load.

8.4. Solution time

The meshing algorithm in ANSYS® allows the degree of mesh coarseness to be selected by the analyst. Mesh coarseness is measured on a scale from 1 to 10, with 10 being the coarsest mesh. As mesh coarseness is reduced more elements are created. A finer mesh results in the boundary of the body in the model being closer to the actual shape of the body, and this reduces the effect of stress concentrations due to meshing. However, a finer mesh also increases the number of elements used, which results in longer solution times (Fig. 12).

Figure 12 indicates that the time to find T_{all} for a particular rigging case increases dramatically below coarseness level 7. The problem of increasing solution time is even more dramatic when the model is being used for parameter analysis. For example, a small parameter analysis may result in 200 rigging cases. At mesh coarseness level 7, 200 rigging cases would take 20 days, whereas at mesh coarseness level 5, 200 rigging cases may take 100 days.

8.5. Allowable skyline tensions

In this section the T_{all} calculated using the two algorithms developed to search for σ_{max}, method 1 and method 2, will be compared. As noted in section 7, method 1 was sensitive to the coarseness of the meshing (Fig. 13). In Fig. 13, T_{all} increases as the meshing coarseness decreases except for a slight wobble, which is most noticeable at mesh coarseness level 6. It is unclear at this time whether the decrease in T_{all} at mesh coarseness level 6 is a function of the body shape resulting from the meshing level or whether it is a result of a change in the solution algorithm used in ANSYS® to solve larger models; however, in the following, consideration of method 2 will add some clarity. The difference in T_{all} between mesh coarseness level 6 and mesh coarseness level 5, as a percentage of the mesh coarseness level 5 value, ranges between 5.1% and 7.5% for the rigging cases considered when using method 1. The difference in T_{all} between mesh coarseness level 10 and mesh coarseness level 5, as a percentage of the mesh coarseness level 5 value, ranges between 17.9% and 27.4% for the rigging cases considered when using method 1.

Method 2 was found to be less sensitive to meshing coarseness (Fig. 14); however, there is still a noticeable drop in T_{all} at mesh coarseness level 6. If method 2 is used, the magnitude of the drop at mesh coarseness level 6 is much less than when method 1 is used. The difference in T_{all} between mesh coarseness level 6 and mesh coarseness level 5, as a percentage of the mesh coarseness level 5 value, ranges between 0.6% and 4.3% for the rigging cases considered. It is interesting to note the decrease in T_{all} at mesh coarseness level 6 is less noticeable for the rigging configurations that resulted in lower T_{all} values.

Recall from section 8.2 that the rigging configurations with lower T_{all} values were dominated by bending, and so σ_{max} occurred well away from the upper boundary of *B*. Note in Fig. 10 that there is higher fluctuation in the normal stress on the transverse cross section near the upper boundary of *B*, and that the magnitude of the fluctuation is dependent on the mesh coarseness level. It is interesting to note that this fluctuation was greater at mesh coarseness level 6 than at 7, and as already noted it is unclear whether this is a function of the meshing algorithm or the solution algorithm in ANSYS®. This indicates mesh coarseness level 6 is not a good choice for stiff backspars.

Figure 14 demonstrates there is a dramatic reduction in the effect that mesh coarseness has on calculating T_{all} when using method 2. The difference in T_{all} between mesh coarseness level 10 and mesh coarseness level 5, as a percentage of

Fig. 14. Allowable tension in the skyline strap (T_{all}) calculated using method 2.

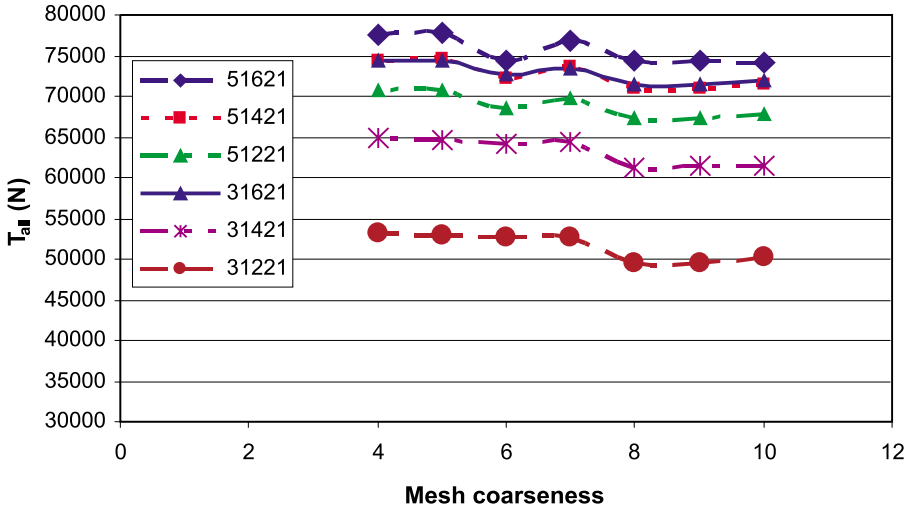

Fig. 15. The ratio of T_{all} (allowable tension in the skyline strap) calculated using method 2 to T_{all} calculated using method 1.

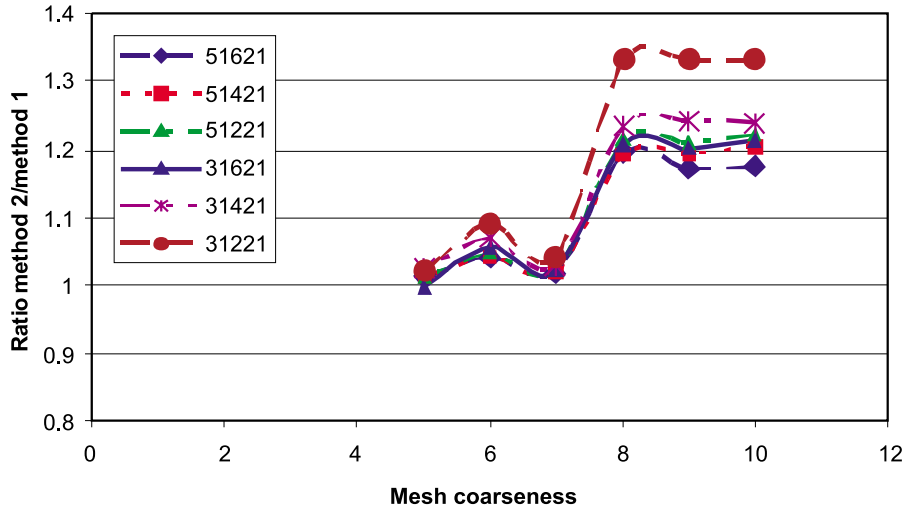

the mesh coarseness level 5 value, ranges between 3.3% and 5.2% for the rigging cases considered when using method 2. Recall from section 8.4 that the solution times were dramatically lower at mesh coarseness level 7 than at mesh coarseness level 5. The difference in T_{all} between mesh coarseness level 7 and mesh coarseness level 5, as a percentage of the mesh coarseness level 5 value, ranges between 0.5% and 1.3% for the rigging cases considered when using method 2. This indicates for the rigging cases considered in this study that using mesh coarseness level 7 and method 2 would be most efficient.

If the difference in T_{all} between method 1 and method 2 is a function of mesh coarseness, then the ratio of T_{all} calculated using method 2 to T_{all} calculated using method 1 should approach unity as the mesh coarseness decreases (Fig. 15).

9. Conclusions

This study indicates that the backspar system can be modeled with solid elements using the commercial software ANSYS®. Numerical solution of the model stabilized at mesh coarseness levels that produce solutions for a given rigging configuration in a reasonable amount of time (0.1 days at mesh coarseness 7). In this study an iterative routine was developed to find T_{all}, and this routine was found to converge rapidly from initial values that were below and above the allowable skyline strap tension.

In the analysis performed in this study the plane that the backspar displaced in was known a priori because of the symmetry of the rigging. A priori knowledge of the plane that the backspar displaced in permitted the use of the method 2 search for σ_{max}. The method 2 search for σ_{max} was less sensitive to mesh coarseness, with at worst only a 5.2% difference in T_{all} from mesh coarseness level 10 to mesh coarseness level 5. When the calculation time for a solution is considered, this study indicates it is most efficient to use mesh coarseness level 7 and method 2 to calculate T_{all}.

The analysis of the modeling results from this study indicates there are two classes of backspars. One class where σ_{max} is dominated by bending and a second class where σ_{max} is dominated by axial compression. This finding has important implications in modeling backspars and in the development of rigging guidelines.

10. Future work

Further model development must include consideration of the cable connections to the backspar and anchors. Improved modeling of the cable connections to the backspar is important when considering the stress concentration resulting from simply connecting the cables to nodes on the surface of the backspar. It was found that the stress concentrations due to simplified cable connections were not significant for rigging configurations where σ_{max} is dominated by bending. However, for rigging configurations where σ_{max} is dominated by axial compression it becomes difficult to isolate the stress concentrations due to the simple cable connections. Therefore, to accurately model stiff backspars it will be necessary to improve the cable connection model to reduce the stress concentrations.

Further work will also be required to determine allowable stress values for the wood in live trees. These allowable stress values will have to be specific to the two backspar classes identified in this study.

Acknowledgements

The authors gratefully acknowledge the assistance provided by the province of British Columbia through the Forestry Innovation Investment Program, and the access to the ANSYS® software through the ANSYS Education Program.

References

American Forest and Paper Association. 1997. National Design Specification (NDS), Supplement for wood construction. American Forest and Paper Association, American Wood Council, Washington, D.C.

Ammeson, J.E., Pyles, M.R., and Laursen, H.I. 1988. Three-dimensional analysis of guyed logging spars. Comput. Struct. **29**(6): 1095–1099.

Bodig, J., and Jayne, B.A. 1993. Mechanics of wood and wood composites. Krieger Publishing Company, Melbourne, Fla.

British Ropes. 1955. Wire rope hand book and catalogue. British Ropes Canadian Factory Limited, Vancouver, B.C.

Carson, W. 1977. Analysis of the single cable segment. For. Sci. **23**(2): 238–252.

Connor, G.F. 1989. Comparison of field-test and computer-model results for a 3-D guyed logging spar. M.Sc. report, Department of Civil Engineering, Oregon State University, Corvallis, Ore.

Conway, S. 1976. Logging practices: principles of timber harvesting systems. Miller Freeman Publications, San Francisco, Calif.

Kozak, A. 1988. A variable-exponent taper equation. Can. J. For. Res. **18**: 1363–1368.

Lyons, C.K. 1997. Analysis of line tensions and backspar stresses in a skyline system: a pilot study. Forest Engineering Research Institute of Canada, Vancouver, B.C. Tech. Note TN-258.

Lyons, C.K., Guenther, R.B., and Pyles, M.R. 2002*a*. Elastic equations for a cylindrical section of a tree. Int. J. Solids Struct. **39**: 4773–4786.

Lyons, C.K., Guenther, R.B., and Pyles, M.R. 2002*b*. Considering heterogeneity in a cylindrical section of a tree. Int. J. Solids Struct. **39**: 4665–4675.

Pellicane, P.J., and Nilson, F. 1993. Three-dimensional model for wood-pole-strength predictions. J. Struct. Mech. **119**(7): 2199–2214.

Pyles, M.R. 1987. Structural properties of second-growth Douglas-fir logging spars. Trans ASAE (Am. Soc. Agric. Eng.), **30**(1): 65–69.

Pyles, M.R., and Lyons, K. 2001. Analysis of unguyed spar trees. Int. J. For. Eng. **12**(2): 11–17.

Schneigert, Z. 1966. Aerial tramways and funicular railways. Pergamon Press, London.

Stalnaker, J.J., and Harris, E.C. 1989. Structural design in wood. Van Nostrand Reinhold, New York.